Master's Thesis in Graduate School of Library, Information and Media Studies

# 3D Auxetic Structure of Ron Resch Pattern using 2D Plane Processing Machine

March 2022

201821608

Uzawa Shingo

# 3D Auxetic Structure of Ron Resch Pattern using 2D Plane Processing Machine

# 2次元平面加工機によるロンレッシュパターンを用いた3次元オーセティック構造

Student No.: 201821608
氏名：鵜沢　信吾
Name: Uzawa Shingo

Auxetic structures and auxetic smaterials are structures with negative Poisson's ratios, which behave in the opposite way to natural materials with positive Poisson's ratios. It is a material that expands using elastic deformation. Auxetic structures have been studied as scalable geometries because there are various geometries with negative Poisson's ratio in three dimensions by three-dimensional deformation. However, most of these studies are based on the premise that 3D printers are used for manufacturing. Since manufacturing constraints affect the cost of equipment and materials as well as manufacturing time, auxetic structure is rarely chosen as a structural option for the actual manufacturing of a product. Therefore, in this paper, propose a model "3D Auxetic Structure of Ron Resch Pattern using 2D Plane Processing Machine", which can be fabricated by planar machining of the 3D Auxetic structure already proposed. In the proposed structure, a three-dimensional auxetic structure can be created using only a two-dimensional machining tool by combining the existing structure created by planar machining. The proposed structure was analyzed and tested based on the results of Poisson's ratio, bistability, and load-displacement curves to demonstrate its properties as a complementary auxetic structure.

Main Academic Advisor: Yoichi OCHIAI
Secondary Academic Advisor: Tatsuki FUSHIMI

# 3D Auxetic Structure of Ron Resch Pattern using 2D Plane Processing Machine

**Uzawa Shingo**

**Graduate School of Library, Information and Media Studies**

**University of Tsukuba**

**March 2022**

# Contents

# List of Figures

# List of Tables

# Chapter 1

# Introduction

## 1.1 Background

Natural materials generally have a positive Poisson's ratio. On the other hand, the auxetic structure has a negative Poisson's ratio. A negative Poisson's ratio means that it stretches in the direction perpendicular to the tensile force and contracts in the direction perpendicular to the load. The auxetic structure is used for façade where the volume of the product can be compressed and expanded, and the size of the opening can be adjusted. As shown in [7], there are various application examples, such as an expansion of table area and packing design.

The study of materials with negative Poisson's ratio dates back to 1985 by A.G. Kolpakov, "Determination of the average characteristics of elastic frameworks." In 1987, R. S. Lakes of the University of Wisconsin-Madison published a paper in SCIENCE entitled "Foam structures with a Negative Poisson's Ratio" [8]. The term "combustible material" was coined in 1991 by Dr. Ken Evans of the University of Exeter [9]. After that, advances in 2D processing machines such as laser cutters and digital fabrication technology such as 3D printers made it possible to manufacture complex shapes, and many auxetic structures with three-dimensional deformation characteristics that could not be made until then became possible. As one of them, a structure based on a rotating polygon, as shown in Figure 7 of [10] has been proposed. However, this structure is a proposal as a scalable geometric shape, and the application of the structure to the scale of architecture and products has not been studied. Therefore, in order to explore the applicability of this scalable geometric shape in relatively large structural designs such as furniture design and architecture at the expense of fine workability, in this thesis, a model that can be manufactured with a two-dimensional processing machine is used.

## 1.2 Research Motivation

The purpose of this study is to realize auxetic structure with a negative Poisson's ratio in three dimensions by processing only two-dimensional planes. To achieve this goal, we combined a square Ron Resch pattern with a negative Poisson's ratio with respect to the XY axis and a cylindrical twist-fold, which is an origami structure that collapses while twisting.

The square Ron Resch pattern and the cylindrical twist fold are both planar structures. When they are combined while keeping the degree of freedom of deformation and the orbits

consistent, the Ron Resch pattern expands in the XY axis while the cylindrical twist-fold expands in the Z axis, thus realizing a three-dimensional auxetic material.

However, twist-folding structure cannot be compressed unless flexure is allowed in the deformation process. Thus, a structure called LETA was adopted, in which a rigid body is given elasticity by applying a two-dimensional cut pattern.

In this thesis, experimental and analytical values of the load-displacement curve, trajectory of deformation, bistability, and Poisson's ratio are presented for the proposed structure, and the results are discussed.

## 1.3 Proposal of This Research

The structure of this paper is as follows. Chapter2 summarizes related studies and presents the position of this structure; Chapter3 presents the principles pf the three types of structures used in this structure (LETA, Ron Resch, and Twist Folding); Chapter 4 proposes the method of this study; Chapter 5 presents experimental and analytical results for the load-displacement curve, deformation trajectory of the structure, bistability, and Poisson's ratio; Chapter 6, the results pf Chapter 5 are discussed.

## 1.4 Contribution

The principle model of the structure of the proposed method in this thesis is proposed in [7]. To the best of our knowledge, there is no feasible proposal that assumes the design is done on a two-dimensional machine, although the structure proposed in [7] has been made on a 3D printer. Therefore, in this paper, we proposed a model that can be manufactured by a two-dimensional machine and actually manufactured it, and conducted experiments and analysis.

# Chapter 2

# Related Work

## 2.1 Auxetic structure

This terminology called auxetic structure was coined by K. Evans at University of Exeter from a paper published in 1991 [11]. The earliest research published example of auxetic structure is due to A. G. Kolpakov in 1985 [12], and the next synthetic auxetic structure was published in SCIENCE in 1987 by R. S. Lakes from the University of Wisconsin Madison [8]. The auxetic structure has been shown to have excellent toughness and hardness, as well as vibration and sound absorbing properties [13, 14].

The auxetic structure exists in two-dimensional planar and three-dimensional planar structures. The two-dimensional auxetic structure expands and contracts in the XY plane, and the three-dimensional auxetic structure expands and contracts in the XYZ direction. In two-dimensional and three-dimensional expansion and contraction have three main types of unit geometric structures: Re-entrant structures, Chiral structures and Rotating rigid structures.

The prototype of the Re-entrant structures is shown in [15] and novel model is proposed to explain foams with negative Poisson's ratio and to describe the strain-dependent Poisson's function behaviour of honeycomb and foam materials in [16]. Re-entrant structures are those that are "inwardly oriented" or have a negative angle. Papers [17, 18] in regard to the thermoplastic resin foams as foams with Re-entrant structures, and arrow-shaped [19], spiral-shaped [20], star-shaped [21] as derivative shapes of Re-entrant structures have also been discovered. In [22], there is a model in which Re-entrant structures are arranged at right angles to form a threedimensional expansion. Chiral structures are structures consisting of a central cylinder wrapped in a ligament attached in the tangential direction and are structures that expand and contract the entire structure by expanding and contracting the spirally generated beam by elastic deformation. Its geometric properties are studied in [23]. A shape like [24] has also been discovered as a derivative system. [25] was announced as a three-dimensional model of chiral structures.

Rotating rigid structures first explored its properties in [26]. It is also called the Ron Resch pattern and is used in this structure. In [27, 28, 29, 30, 31], how the Poisson's ratio changes by replacing the unit geometry that composes the Ron Resch pattern from a square to various shapes is studied.

## 2.2 Origami

The structure of origami has various functions. The main functions are high strength, actuation, shape generation, and folding compression [32, 33, 34, 35]. Various studies have been conducted especially on folding compression, such as space industry, fashion, architecture, and MEMS [36, 37, 38, 39, 40, 32, 33, 34]. For folding, Miura-ori [41], cylindrical twist folding [42], and Yoshimura pattern [43] are frequently used as an application. Cylindrical torsional folding was modeled by Nojima [42], and then Ogiwara et al. optimized the crushing deformation characteristics [44] and ZHAO et al. researched the optimum design [45].

Cylindrical torsional folding is a structure in which buckling occurs and is folded in the process of deformation, and Yamaki analyzed the buckling [46]. In this origami structure that requires bending, Yasuda, et al. place a spring that expands and contracts in the direction of the next fold line at the fold line of the twist fold, and research is being conducted to mechanically handle the twist fold [47].

## 2.3 Structure by Two-Dimensional Plane Processing

In two-dimensional plane machining including CNC and laser cutters, attempts are being made to express various expressions from the constraints of the three-axis machining flexibility. Surface processing is used to manufacture curved surfaces [48], deformation control [49], and structures that give elasticity to materials are being sought [5]. The structure that gives elasticity by the cut pattern is also called Array of LET Joint [50], Compliant Arrays [51], and Slit-based material [5]. Oshima, et al. proposed an analysis model of an elastic body formed by using a two-dimensional repeating slit pattern [5]. This structure proposes to allow torsional bending by adjusting the parameters of LETA.

In this study, we propose a new three-dimensional auxetic structure that can be manufactured by two-dimensional plane machining by combining the Ron Resch pattern, which is an auxetic material that can be manufactured by two-dimensional plane machining, and the cylindrical twistfolding structure, which is an origami structure that can be shrunk in the axial direction. By using LETA, a technology that imparts elasticity by repeating cut patterns, twist folding in flat surface processing is realized. With this structure, a structure with a dynamic Poisson's ratio can be manufactured by a relatively inexpensive and general-purpose manufacturing method, and there is a possibility that a large compression of the volume of the product can be expected.

# Chapter 3

# Principle

The principle of the structure used to manufacture this structure by two-dimensional plane processing will be explained.

Section 3.1 explained the Ron Resch pattern, which is the basic structure. Section 3.2 describes the cylindrical twist folding that connects the Ron Resch patterns. Section 3.3 explained the correspondence between the Ron Resch pattern and the cylindrical twist fold. Section 3.4 explain the structure for enabling the deformation of cylindrical torsion with a solid flat plate.

## 3.1 Ron Resch

First, the Ron Resch pattern contributes to the expansion in the X and Y direction. The Ron Resch pattern is an origami pattern discovered by Ron Resch in the 1960s and 1970s. The most typical Ron Resch pattern is shown in Figure 3.7. There are various geometric shapes in the Ron Resch pattern Figure 3.2, and there are various mechanisms to realize, such as origami and link mechanisms. In this structure, a model of the square Ron Resch pattern of the link mechanism is used Figure 3.2(a). The quadrangles used in the Ron Resch pattern form a link mechanism, which causes expansion in the X and Y axes before and after deformation.

In this paper, the Ron Resch pattern is mentioned in various sections, but it is explained using the three words 'square Ron Resch pattern', 'unit cell', and 'square'. Each of them is defined in Figure 3.3.

Various types of the Ron Resch pattern have been announced, and all of them are modified to have a negative Poisson ratio. The rotating square model used in this structure is introduced as a new mechanism by Grima and Evans [2]. This structure is based on the arrangement of rigid squares hinged at the vertices, as shown in Figure 3.4. Concerning equation 3.1, if squares of side length $l$ have an angle $\theta$ with each other, the dimensions of the unit cell are given as follows:

$$x_1 = x_2 = 2l\left[\cos\left(\frac{\theta}{2}\right) + \sin\left(\frac{\theta}{2}\right)\right]. \tag{3.1}$$

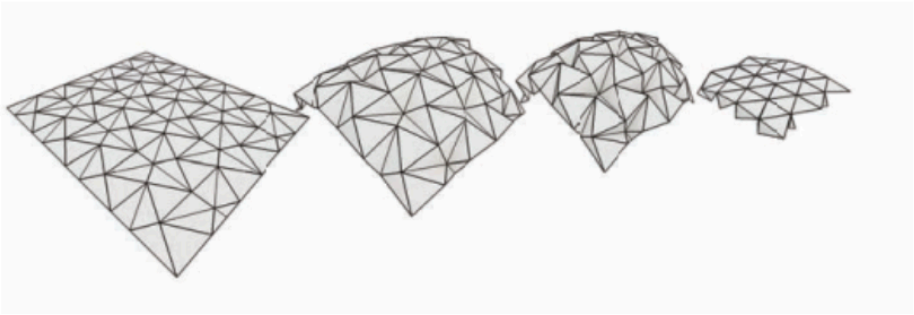

Figure 3.1: Regular triangular tessellation by Ron Resch [41].

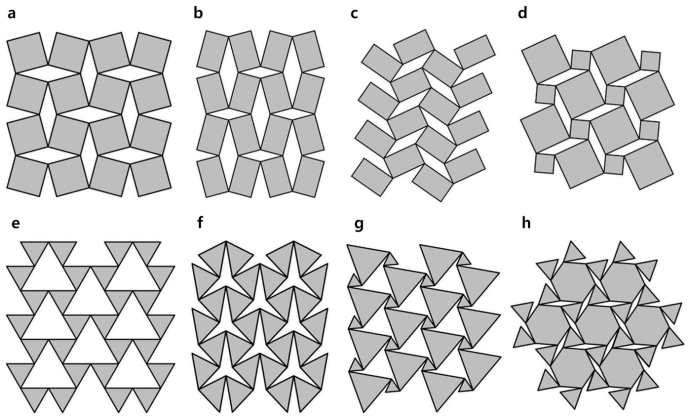


Figure 3.2: Ron Resch patterns with various geometric shapes. (a) is the square Ron Resch pattern used in this structure [1].

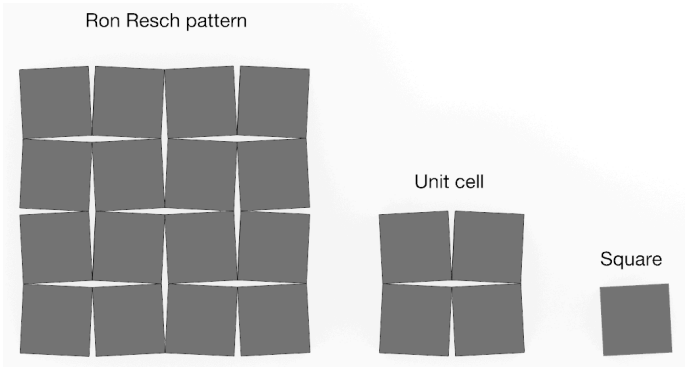


Figure 3.3: Description Shape definition

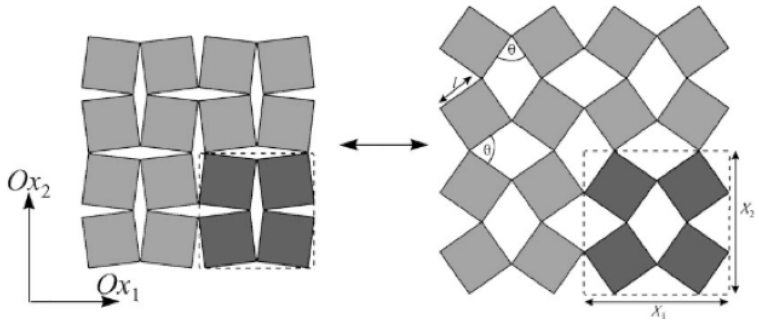


Figure 3.4: Square Ron Resch pattern. The area surrounded by the dotted line is the unit cell [2].

## 3.2 Cylindrical Twist Folding

In this structure, twist folding is used to expand the z-axis direction. Twist folds are sometimes called cylindrical folds or cylindrical twist folds, but they are called twist folds in this thesis.

Twist folding is a pattern that appears naturally when the thin cylindrical shell is compressed while rotating in the axial direction of the cylinder in Figure 3.5. There are various folding angles in the folding pattern as shown in Figure 3.6.

A triangular polygonal line appears when the twisted structure is unfolded as shown in Figure 3.5. Twisting is possible by bending this triangular surface in the process of twisting deformation. The deflection of twist folds is analyzed in "Elastic Stability of Circular Cylindrical Shells." Since twist folding goes through bending once, there are two stable states as shown in Figure 3.8. In twist folding, which can be broken by passing through bending, research is being conducted to allow bending of the surface not only by the surface but also by the axial extension of the polygonal line and to enable folding [47].

In this structure, in order to avoid contact in the process of twist deformation when the thickness of the material is assumed, a structure in which two sides are removed from the folding pattern of the square column is used Figure 3.9. Twist folding is a deformed structure that expands and contracts while twisting on one axis, but in the structure of this study, it contributes to expansion in the Z-axis direction.

In this structure, LETA is used for the polygonal line portion that appears in the developed view of the twisted fold, and the deflection that originally occurs on the surface is absorbed by the LETA, enabling the twisted fold. LETA is described in Section 3.4 .


Figure 3.5: Foldable cylinder based on twist buckling of a paper roll [3].


Figure 3.6: Various geometric shapes of Ron Resch patterns [1].

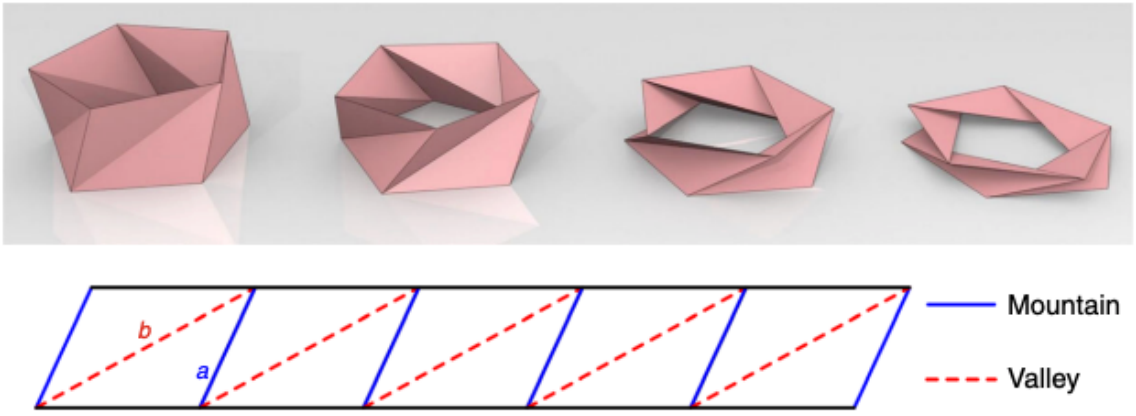


Figure 3.7: Expanded view of a twist folding [4].

[1] https://hamaguri.sakura.ne.jp/oritatami.html

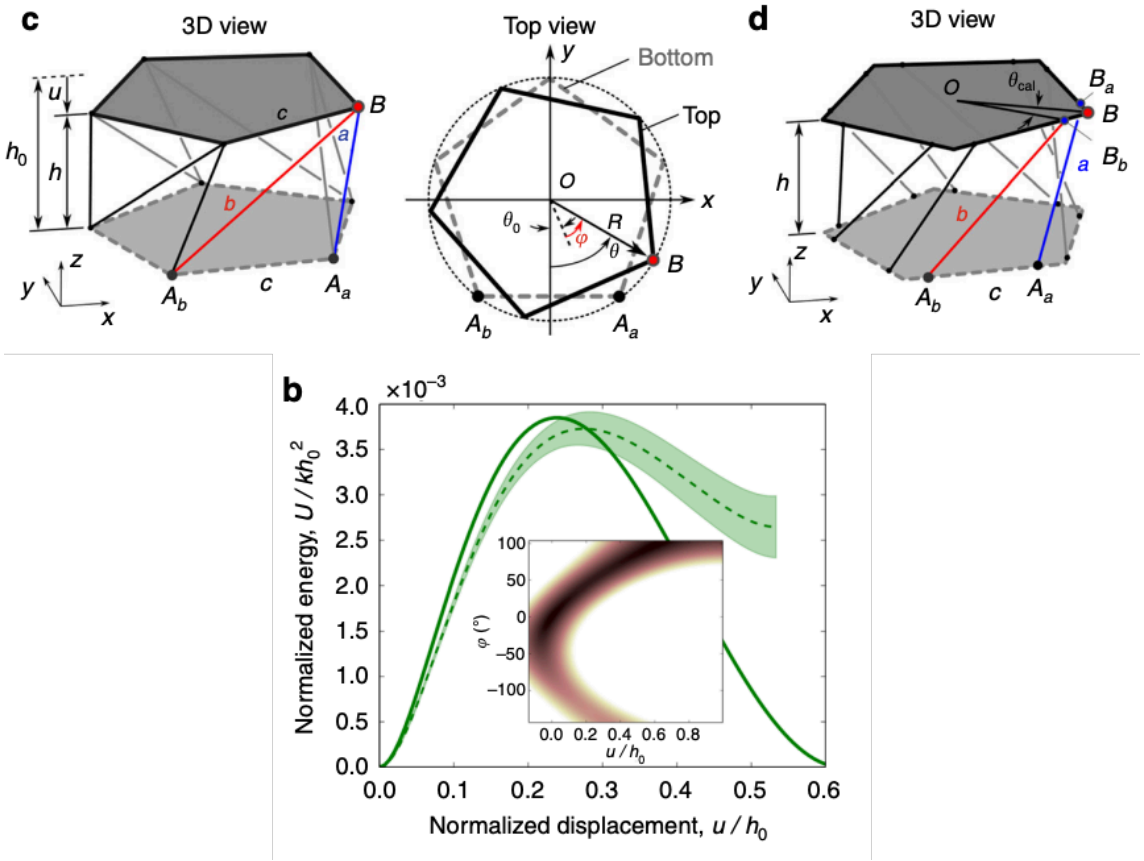


Figure 3.8: Bistability via twist folding deflection. For ($h_0$,$\theta_0$) = (90mm, 46°) [4].

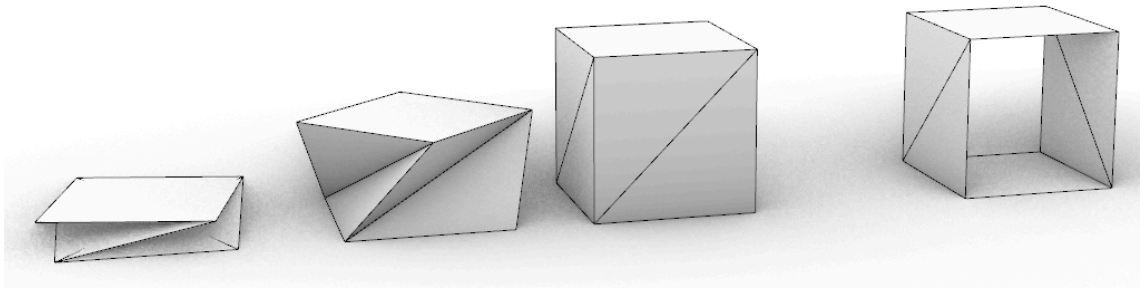

Figure 3.9: Square-column twist folding pattern. The right end is the pattern with the two sides removed from the square column twist folding used in this structure.

## 3.3 Composition of This Structure

The connection relationship of each structure will be explained. In this structure, the Ron Resch pattern is used in the upper and lower parts of this structure, and the upper and lower Ron Resch patterns expand in the X and Y direction while rotating in opposite directions at the same time as shown in Figure 3.10. The quadrangle Ron Resch pattern has a feature that when the square quadrangle constituting the unit cell is a square, the trajectory of the midpoint of the square due to the deformation of the unit cell does not depend on the rotation direction of the deformation of the unit cell. Taking advantage of this symmetry, the prism twist fold and the Ron Resch pattern do not interfere with each other. The upper and lower Ron Resch patterns are connected vertically by twisting a square pillar, which is a rigid origami paper. When the upper and lower Ron Resch patterns are deformed in opposite rotations to each other, this twisting pattern is interlocked and deformed to induce expansion in the z-axis direction.

However, in the proposed structure, because the structure is manufactured by processing a solid flat plate, twist folding cannot absorb the bending. Thus, in the next section, we will explain the principle of LETA, which is a technology for enabling twist folding.

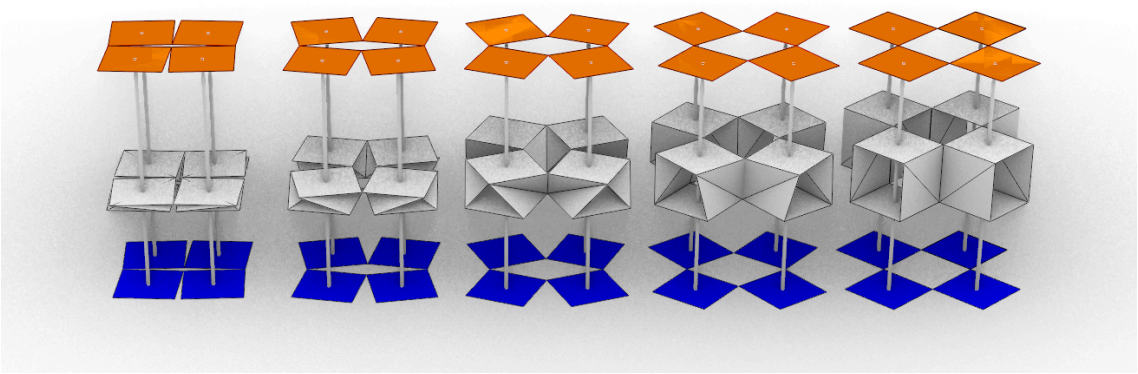

Figure 3.10: Correspondence between the Ron Resch pattern and the twist folding.

## 3.4 LETA

In this structure, LETA was used to realize twist folding only by two-dimensional plane processing of a solid flat plate. LETA is a structure that makes the whole or part of the material a softener by putting a repeated cut pattern on hard material. LETA are mechanical bonding materials that utilize the deflection of a member from a plane to achieve out-of-plane deformation.

In this structure, LETA is used in the twist folding part to absorb the deflection of the twist folding and enable deformation as shown in Figure 3.11.

As shown in Figure 3.12, LETA has four modes: in-plane bending (BIP mode), out-of-plane bending (BOP mode), stretching (S mode), and torsion (T mode). According to the research by Oshima et al. [5], it is possible to derive how much each structural parameter

contributes to the rigidity of each deformation:

$$\text{S-mode} : E\frac{a^3bn}{l^3} \tag{3.2}$$

$$\text{BIP-mode} : \frac{2EIn\left(b^2n^2+\left(n^2-1\right)\left(s^2+2ls\right)\right)}{l^3} \tag{3.3}$$

$$\text{BOP-mode} = (a+g)\,GJ\,(a\cdot h) \tag{3.4}$$

$$\text{T-mode} = \frac{Eal^3\,(a+g)}{l} \tag{3.5}$$

$$J = Torsion\ constant$$
$$G = Shear\ modulus$$

In this structure, LETA's out-of-plane bending mode and twisting mode contribute to the realization of torsional folding. Twist folding is established only by folding in the origami structure. In order to establish this behavior with rigid origami paper, LETA is embedded only in the place where the deformation mode beyond the operation of breaking the fold line is to be obtained, and twisting and stretching are allowed.

Figure 3.11: Correspondence between the Ron Resch pattern and the twist folding.

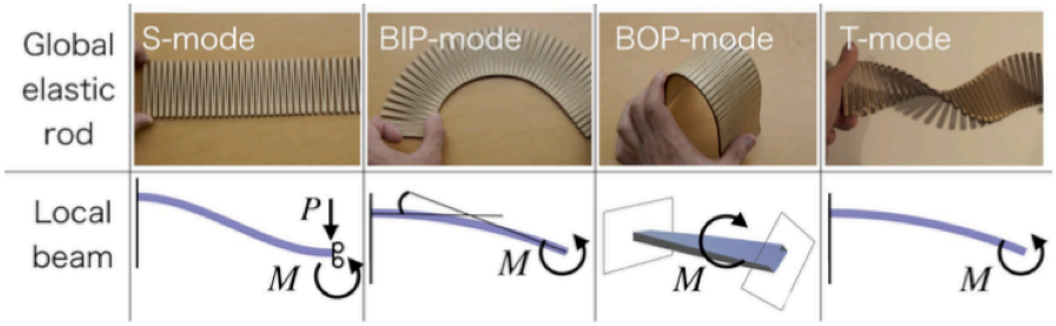


Figure 3.12: The four LETA modes shown in [5, 6].

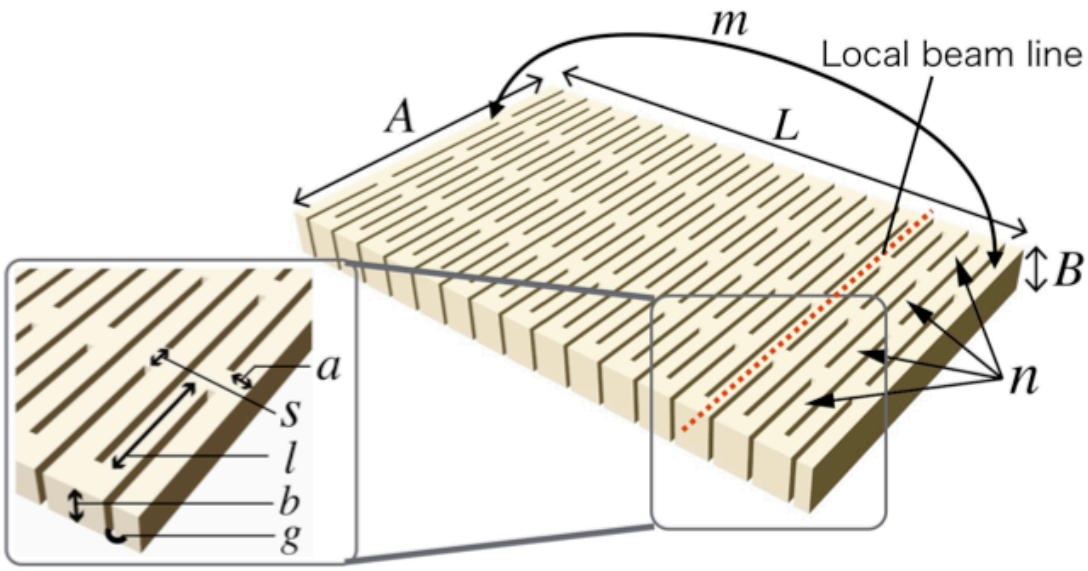


Figure 3.13: Parameters of LETA shown in [5, 6].

# Chapter 4

# Method

The proposed method in Figure 4.1 of this study will be explained. Section 4.1 describes the design, manufacture and assembly of this structure. In Section 4.2, the transformation process and transformation branching of the proposed method are explained.

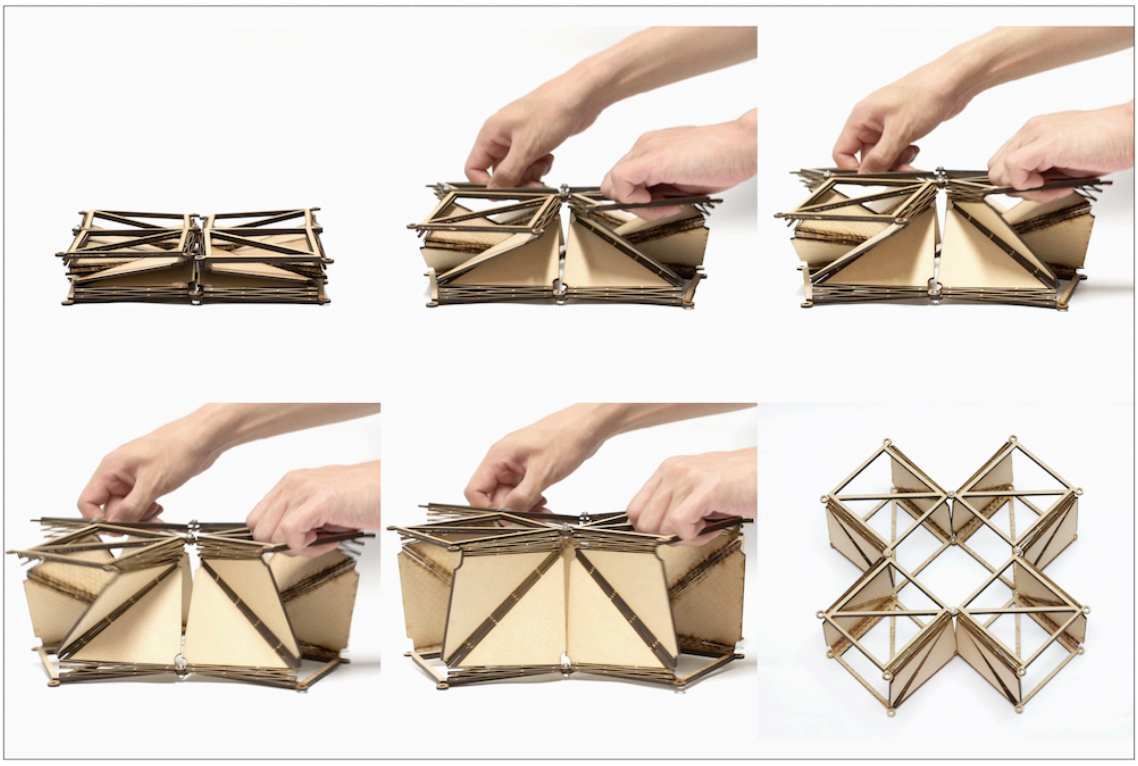

Figure 4.1: The process of deformation of this structure.

## 4.1 Fabrication

Figure 4.2 is an developed view of the structure of the proposed method. Since the developed view of this structure is a deformation realized by combining the structures that can be realized by plane processing, the drawing can be expressed by a plan view. In this paper, a laser cutter was used as the surface processing machine to manufacture this drawing.

In this thesis, the unit shown in Figure 4.3 is called "voxel." The dimensions of the cut drawing in Figure 4.2 are designed so that the bounding box will be 100x100x100[mm] when assembled into this voxel. The area of the blue line shown in Figure 4.2 corresponds to the hole in the blue area of Figure 4.3. Usually, if it is a solid flat plate, the deformation of the structure works. However, this time, to improve the visibility of the internal state during the three-dimensional deformation, a hole is made within the range that does not affect the behavior due to the deformation. The cut boards glue the sides of the structure shown in Figure 4.4 to assemble one voxel. After that, parts were attached to the voxels to make the voxels function as a link mechanism as shown in Figure 4.4. Finally, the voxels were connected to each other with M4 bolts.

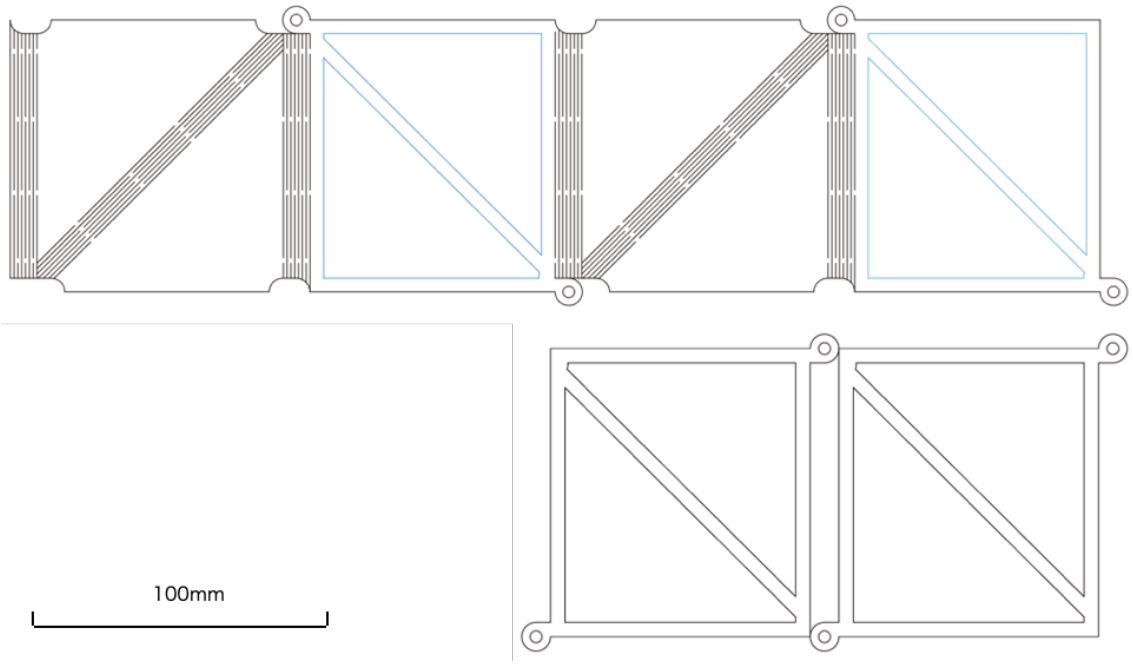


Figure 4.2: Net drawing of the structure

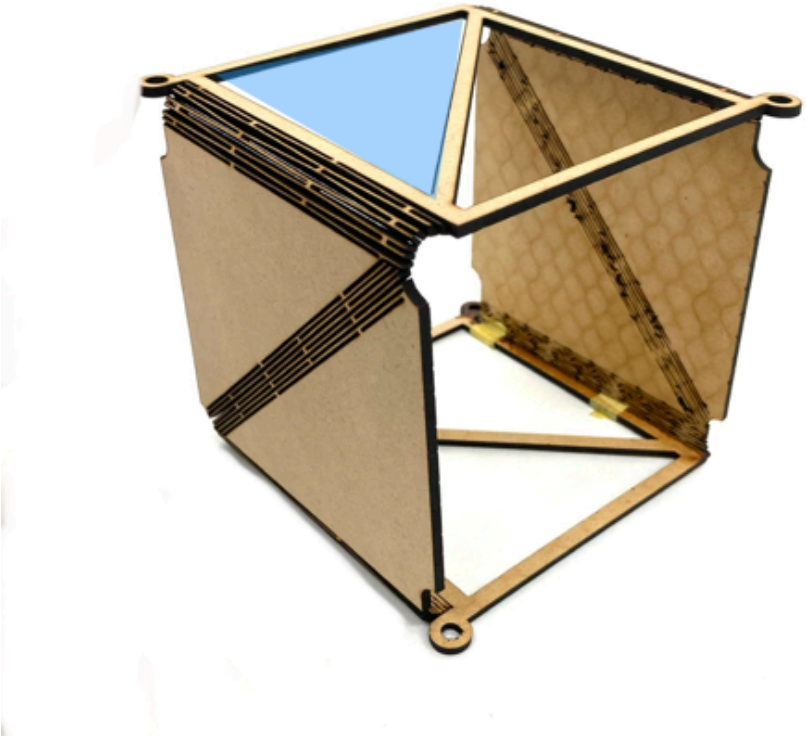

Figure 4.3: Voxel assembled from a laser-cut drawing with an outline of 100 mm square. The holes in the blue area correspond to the blue cut lines in Figure 4.2.

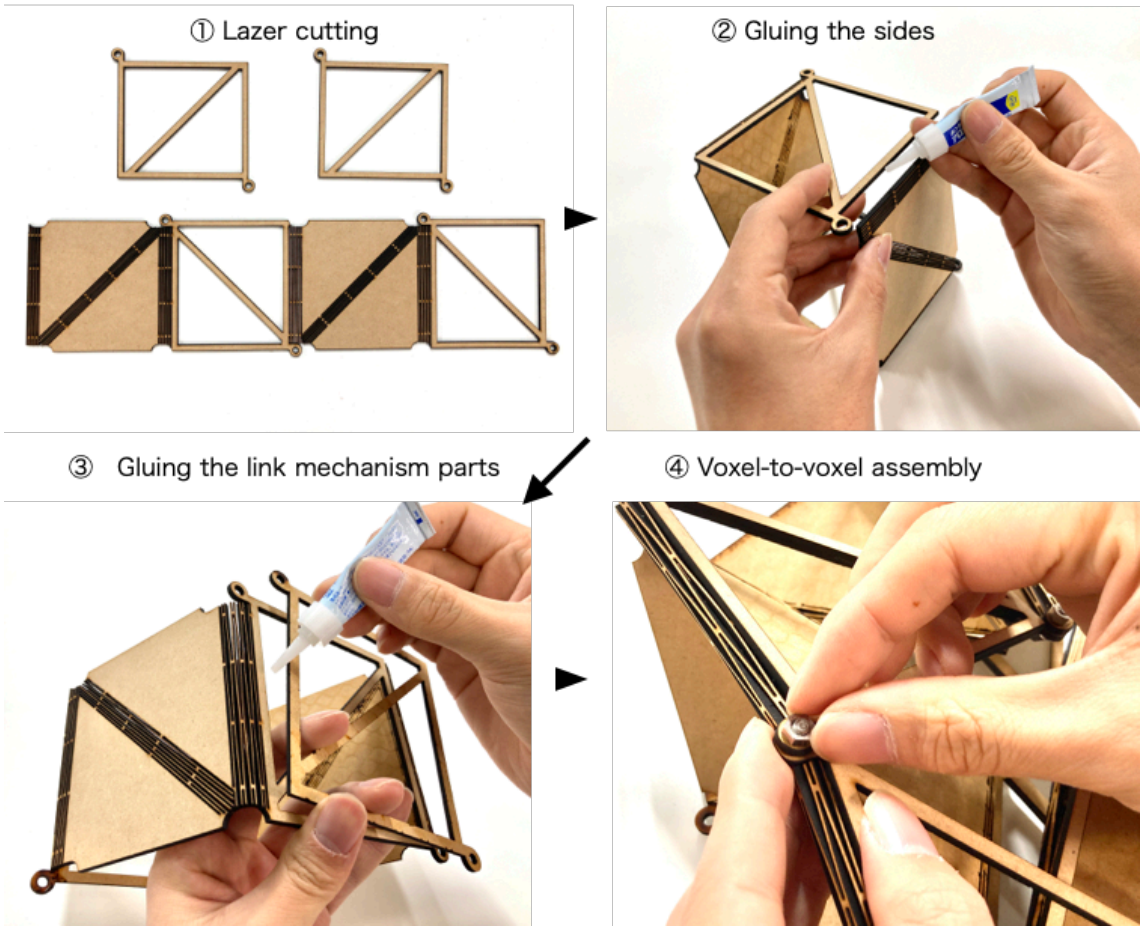


Figure 4.4: Assembly process of this structure.

## 4.2 LETA Parameter

The LETA is used as the structure that bears the hinge part of this structure must reach at least 180°, which is the maximum bending angle before and after deformation, without breaking. In order to find a parameter that satisfies this constraint, the values of four parameters $\{a, b, s, g\}$ among the LETA parameters $\{l, n, a, b, s, g\}$ shown in Figure 4.5 are fixed. The values of the two parameters $\{l, n\}$ are variable. $l$ is variable in the range of 11 mm to 25 mm, and $n$ is variable in the range of 3 to 7. Then, a deformation experiment was conducted in which the LETA was bent 180° while changing the values of $l$ and $n$ (Figure 4.6, 4.7). MDF 2.5mm was used as the material for LETA. As a result of the experiment, it was possible to bend without breaking with the parameters (5) and (6) in Table 4.1. Thus, in the experiments in this chapter, this structure was used for LETA manufactured with the parameter (6).

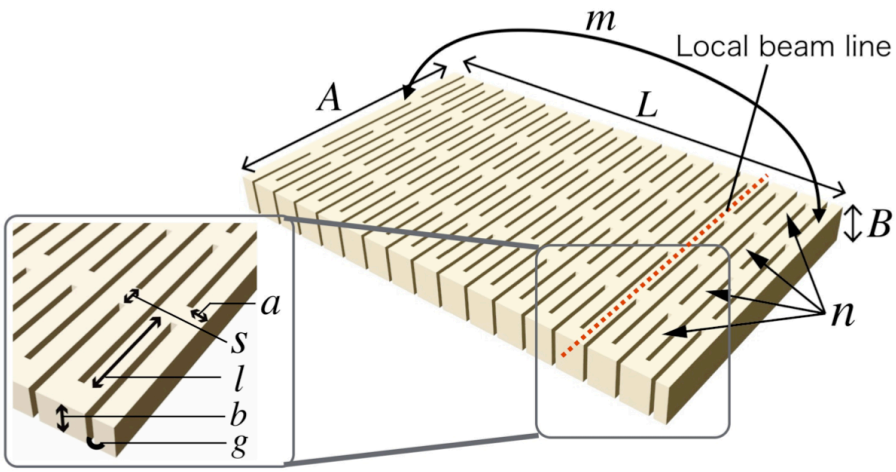


Figure 4.5: Designing parameters for LETA.[51]

Table 4.1: Parameters used in the bending experiment of LETA.

| | ① | ② | ③ | ④ | ⑤ | ⑥ |
|---|---|---|---|---|---|---|
| **l** | **11 [mm]** | **13.5 [mm]** | **16 [mm]** | **18.5[mm]** | **22 [mm]** | **25 [mm]** |
| **n** | **7** | **5** | **5** | **3** | **3** | **3** |
| **a** | 1.4 [mm] | 1.4 [mm] | 1.4 [mm] | 1.4 [mm] | 1.4 [mm] | 1.4 [mm] |
| **b** | 2.5 [mm] | 2.5 [mm] | 2.5 [mm] | 2.5 [mm] | 2.5 [mm] | 2.5 [mm] |
| **s** | 2 [mm] | 2 [mm] | 2 [mm] | 2 [mm] | 2 [mm] | 2 [mm] |
| **g** | 0.3 [mm] | 0.3 [mm] | 0.3 [mm] | 0.3 [mm] | 0.3 [mm] | 0.3 [mm] |

Figure 4.6: Bending experiment of LETA.

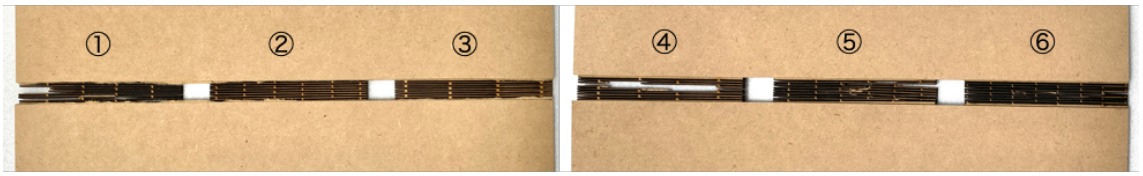


Figure 4.7: A result of bending experiment from Fig4.7. ①②③④ has been broke.

## 4.3 Deformation Mode

As the deformation mode of this structure, a combination of a Ron Resch pattern and a twist-folding deformation mode appears. The theoretical value of the degrees of freedom of the square Ron Resch pattern is one degree of freedom, and twisting and folding is also one degree of freedom if bending is not taken into consideration. (It is a quasi-one degree of freedom when considering that the deflection is ideally absorbed in each surface). Since these freedoms are linked, this structure also has one degree of freedom, but the deformation mode has branches, as shown in Figure 4.8.

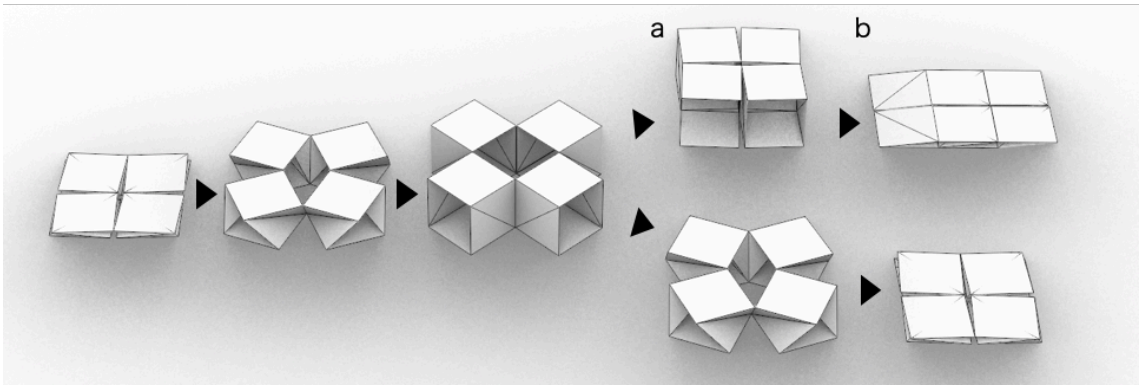


Figure 4.8: Deformation mode of this structure.

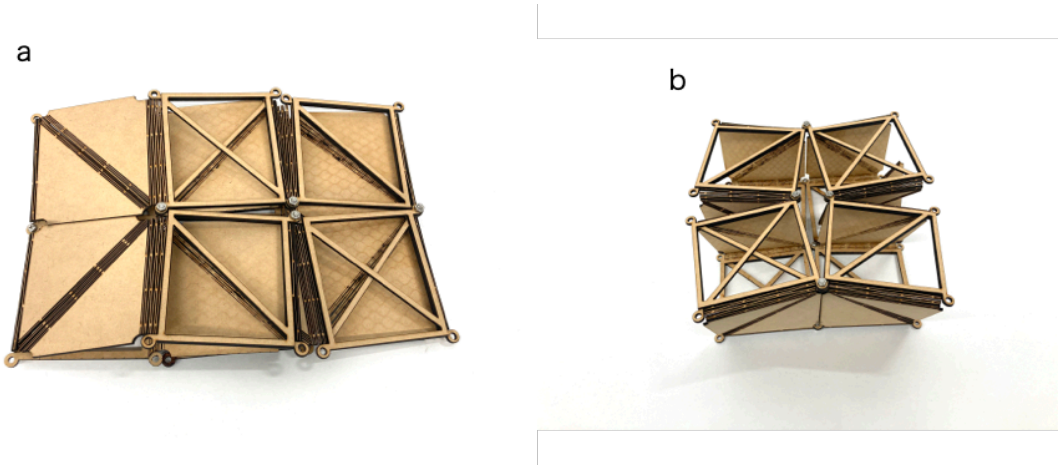


Figure 4.9: Reproduced with the actual structure from a and b in Figure 4.9.

# Chapter 5

# Simulation and Experiment

In this chapter, the characteristics of the structure are evaluated from the analytical values and experimental values in the following four items:

- Displacement for load
- Bistability
- Poisson's ratio
- Trajectory of structural deformation

## 5.1 Load Displacement Curve

In order to evaluate the displacement with respect to the load in the Z-axis direction when the structure is deformed, a finite element method analysis and an experiment using a load tester were conducted. In this section, a load-displacement curve is created, and the graphs of the analytical and experimental values are compared to discuss the error between the two values in Chapter 6.

To show the analysis values of the load-displacement curve, ANSYS, which is a group of analysis software centered on the finite element method, was used. In this structure, one voxel as shown in Figure 4.3 is responsible for the twist-folding structure, and when four voxels are connected by a link mechanism, the deformation behavior of the Ron Resch pattern appears, and it becomes the minimum structural unit of the proposed structure. In this simulation, in order to complete the analysis of one voxel, the geometric constraint condition similar to that when composed of four voxels is given as the boundary condition of the analysis by using the geometric symmetry of the proposed structure. Boundary conditions and material constants were set as follows and analyzed (Figure 5.1):

- A forced displacement of 100 mm was given in the Z-axis direction.
- Bottom B is fixed.
- The center point C on the upper surface is given a degree of freedom only on the axis A.
- Contact between beams inside LETA is not considered.
- The weight of the structure itself is not taken into consideration.
- The Young's modulus of MDF is 3.654 GPa, and the Poisson's ratio is 0.25.

The analysis result is the blue graph shown in Figure 5.2.

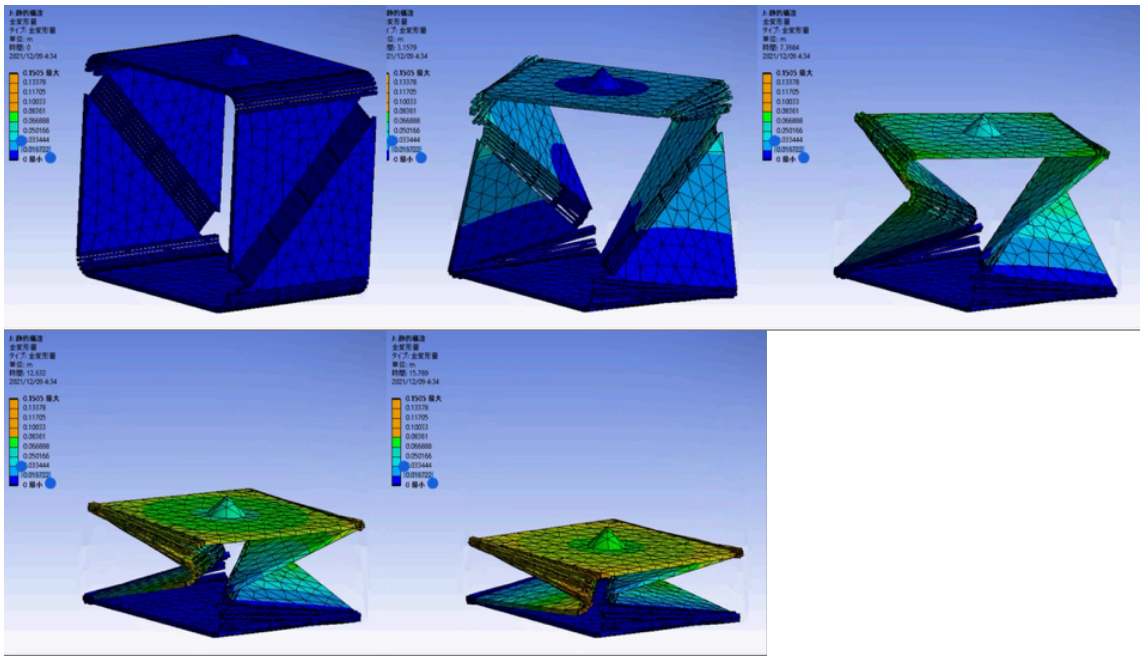

Figure 5.1: Finite Element Method Analysis of Voxels.

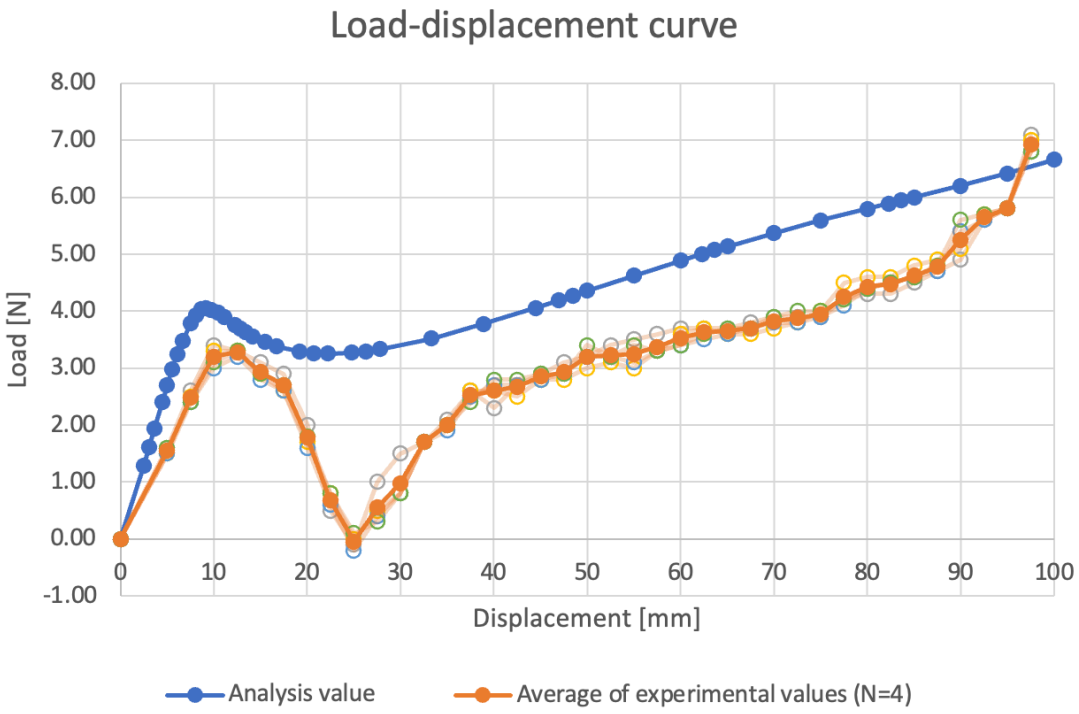


Figure 5.2: Load-displacement curves of analytical and experimental values.

Next, the experimental values were measured. A load tester (AND MCT 1150) was used for the measurement. For the structure used in the load test, the same boundary conditions were reproduced from the analysis performed in Section 5.1, and an experiment with one voxel structure was performed. A rotation mechanism using bearings having a degree of freedom of rotation in the XY plane was attached to the load tester as shown in Figure 5.3. This mechanism allows the degree of freedom of rotation of twisting and bending when a load is applied to the voxel in the Z-axis direction, and compression occurs in the same axis. A voxel was attached so that the center point of the rotation mechanism corresponds to the center point of the upper surface of the voxel structure (Figure 5.4). The bottom surface of the voxel was also adhesively fixed to the load tester so that the boundary conditions were the same as the analysis conditions. The parameters of this structure used in the weighted test are also equivalent to the analysis. In the weighted test, the voxels were installed in a load tester with the voxels fully open, displaced by 2.5 mm in the Z-axis direction, and the reaction force [N] at that time was measured and graphed. The result is the orange graph as shown in Figure 5.2.

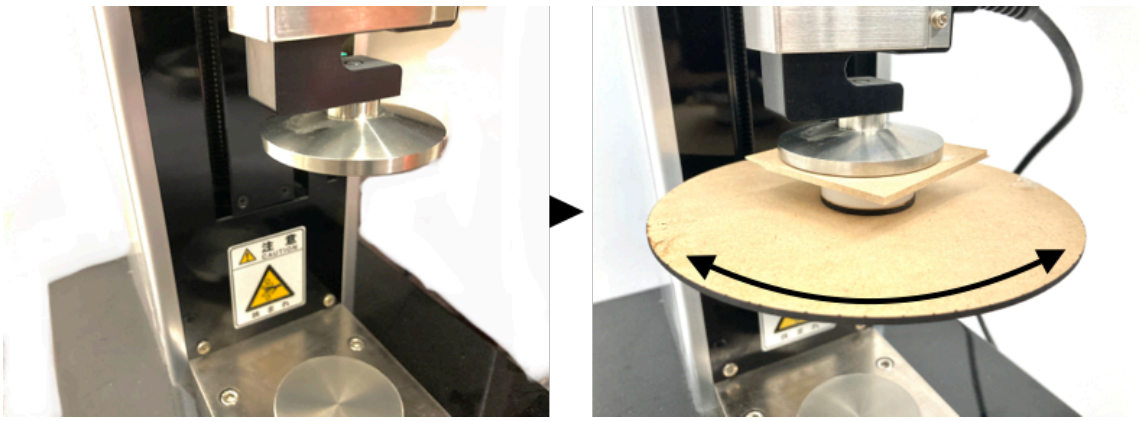

Figure 5.3: The measuring instrument used in the load test. The disk rotates in the direction of the arrow (in-plane).

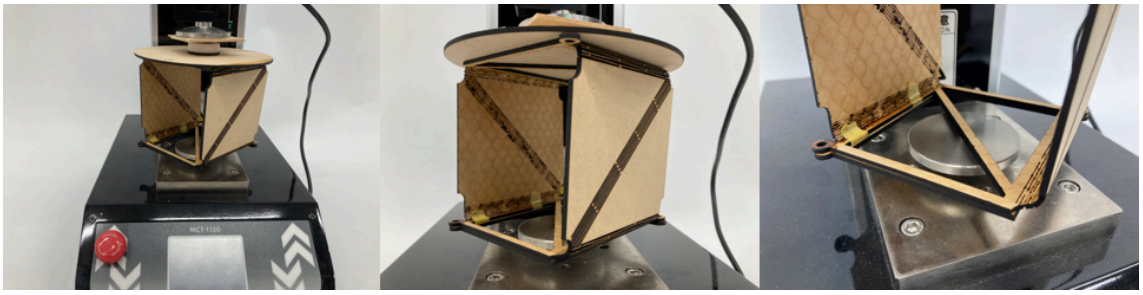

Figure 5.4: Environment for the load test. The voxel is glued to the load testing machine.

## 5.2 Structural Deformation Trajectory

The deformation of this structure is linked to the deformation due to the Ron Resch pattern in the XY plane and the deformation of the torsional fold in the Z-axis direction. In order to investigate the deformation of the Ron Resch pattern corresponding to the deformation of the torsional fold due to the load in the Z-axis direction, a finite element method analysis and a measurement experiment by motion capture were conducted. In this section, a graph of the angle of rotation with respect to the displacement in the Z-axis direction is created, and the error between the two is discussed by comparing the analytical and experimental values in Chapter 6.

#### Finite Element Method Analysis

In order to show the rotation angle with respect to the displacement in the Z-axis direction, the deformation trajectory was analyzed by ANSYS's finite element method analysis under the same analysis conditions as in Section 4.2. A forced displacement of 100 mm was applied to the wholly opened voxel to cause twist-fold deformation, and the trajectory of point is measured to analyze as shown in Figure 5.5. The result is the blue graph in Figure 5.6.

#### Motion Capture

In order to show the trajectory of the deformation of this structure as an experimental value, measurement by motion capture was performed. A marker for observation by motion capture was set at point A as shown in Figure 5.5, and a voxel was installed on the load tester. The voxel boundary conditions for the load tester are the same as those for the load test in Section 5.1. From the fully open state of the voxel, a displacement of 5 mm in the Z-axis direction was applied by the load tester, and the rotation angle of the deformation of the voxel at that time was measured. The result is the orange graph in Figure 5.6.

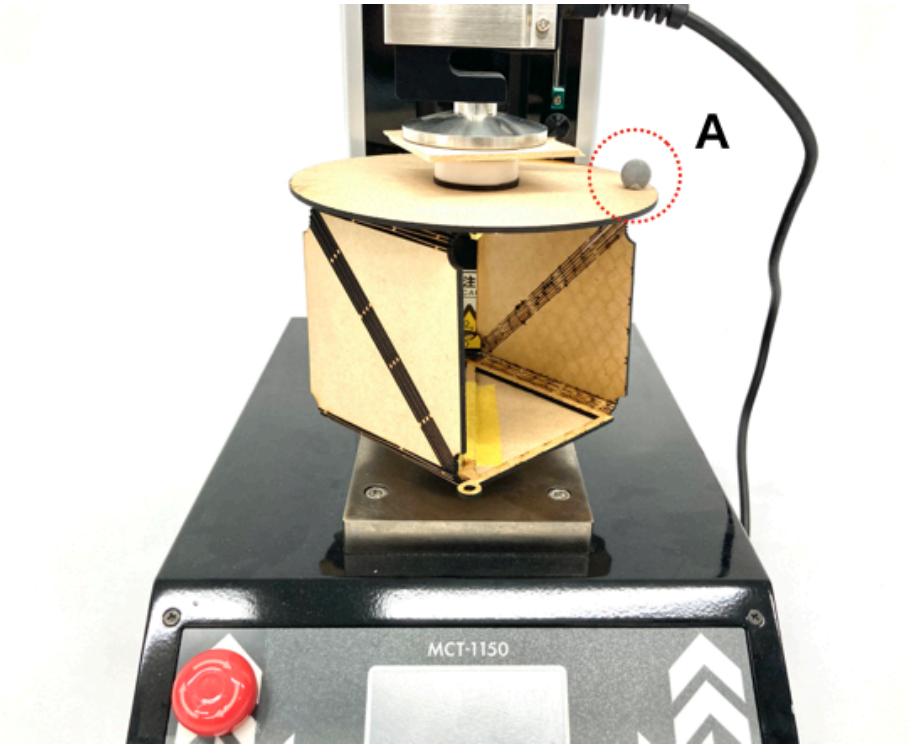


Figure 5.5: Measurement by motion capture. Point A is the observation point.

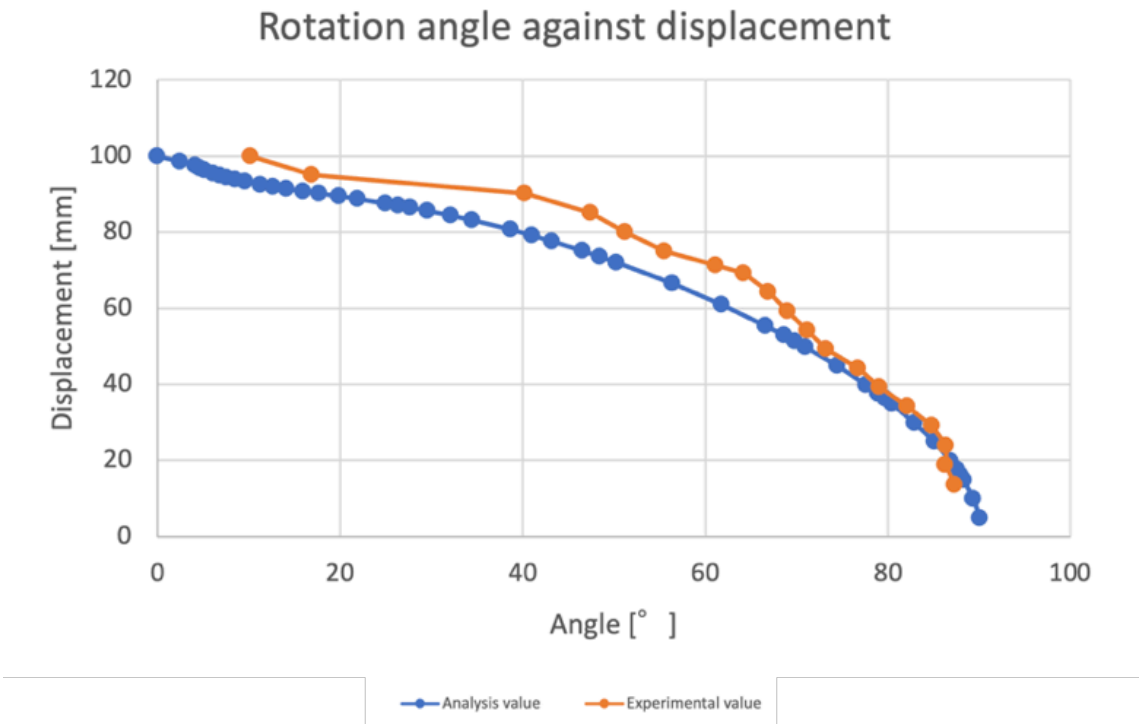


Figure 5.6: Graph of analytical and experimental values of the rotation angle of the structure against displacement.

## 5.3 Bistability and Poisson's Ratio

As described in Chapter 3, the torsional fold used in this structure is deformed via bending so that bistability exists. Even in this structure, the LETA placed on the polygonal line is used as a spring to allow bending. Hence bistability behavior can be seen due to the reaction force of the spring. In this section, to evaluate this structure's bistability, stable state mode A and mode B are shown using the graphs depicted in the finite element method analysis and the experiment with the load tester performed in Section 5.21. Then, the Poisson's ratio between the analysis and experimental values is calculated from the bounding boxes of the stable state modes A and B. Furthermore, the Poisson's ratio from the maximum compressed state of this structure is also calculated regardless of the stable state.

### 5.3.1 Bistability

In the experimental value of the load displacement curve shown in Section 5.1, the stable state mode B is the point where the load becomes 0 for the second time in Figure 5.6. (When the load starts to be applied, the graph moves in the positive direction and later to the negative direction. And the point where the load becomes 0 is the stable state). In the experimental values, the load [N] became 0 when the displacement was 27.5 mm. It is shown by a vertical orange line in the graph. On the other hand, the analysis value did not give a point where the load [N] became 0. However, even in the analysis value, it is assumed that the stable state mode B of the analysis site is the point that first approaches 0 after the load is applied and that is closest to 0. Then, in the stable state mode B of the analysis value, the displacement was 22.2 mm. It is shown by a vertical blue line in the graph. The fact that the load did not reach zero will be discussed in a later section.

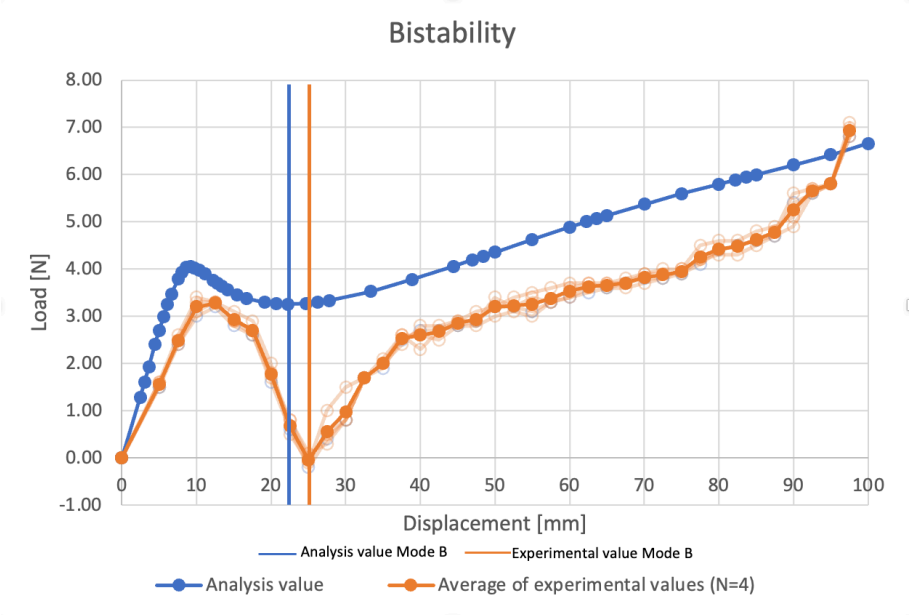


Figure 5.7: Graph of bistability trajectory values calculated from load and displacement versus experimental values.

### 5.3.2 Poisson's Ratio

First, the Poisson's ratio of the experimental value of this structure is calculated. As a method of calculating Poisson's ratio, it is calculated by the extension of the bounding box surrounded by the dotted line as shown in Figure 5.8. The bounding box surrounded by the dotted line appears when the blue square of B, which is a Ron Resch pattern, is rotated around the red point A shown in the lower right of Figure 5.8. Because this structure is three-dimensionally extended, the Poisson's ratio in the XY and YZ planes as shown in Figure 5.8 is calculated. For the YZ plane, since this structure has geometric symmetry, it is assumed to be equivalent to Poisson's ratio in the XZ plane.

First, Poisson's ratio is usually expressed by the following formula:

$$v = -\frac{\varepsilon_d}{\varepsilon_L} \tag{5.1}$$

At this time, $\varepsilon$ is obtained by calculating the vertical strain $\varepsilon_d$ and the horizontal strain$\varepsilon_L$ by the following equations:

$$\varepsilon_d = \frac{\Delta d}{d} \tag{5.2}$$

$$\varepsilon_L = \frac{\Delta L}{L} \tag{5.3}$$

In these equations, assuming that $\varepsilon_z$ is the vertical distortion and $\varepsilon_Y$ is the horizontal distortion, and by substituting the values of the mode A bounding box and the mode B bounding box shown by the dotted line as shown in Figure 5.8, the Poisson's ratio can be calculated:

$$v(xy) = -1$$
$$v(xz) = -0.202$$

The YZ Poisson's ratio was calculated from mode B in the experimental graph. However, when a further load is applied from the displacement reached mode B, the rigid materials come into contact, and the deformation stops as shown in Figure 5.10. Therefore, the Poisson's ratio is also calculated at the position where the deformation has stopped. The bounding box at the position where it stopped due to the contact generated by the deformation of this structure as shown in Figure 5.9. Substituting the values into the equation yielded:

$$v(yz) = -0.046$$

The Poisson's ratio of the analysis value is calculated in the same way as the experimental value. When the bounding box is calculated from the graph of the analysis values shown in Section 5.3, mode B is Y = 258.34 and Z = 77.8. After substituting into the equation, $v(xy)$ and $v(yz)$ can be obtained as follows:

$$v(xy) = -1$$
$$v(yz) = -0.362$$

All calculated Poisson's ratios are rounded up to the fourth decimal place.

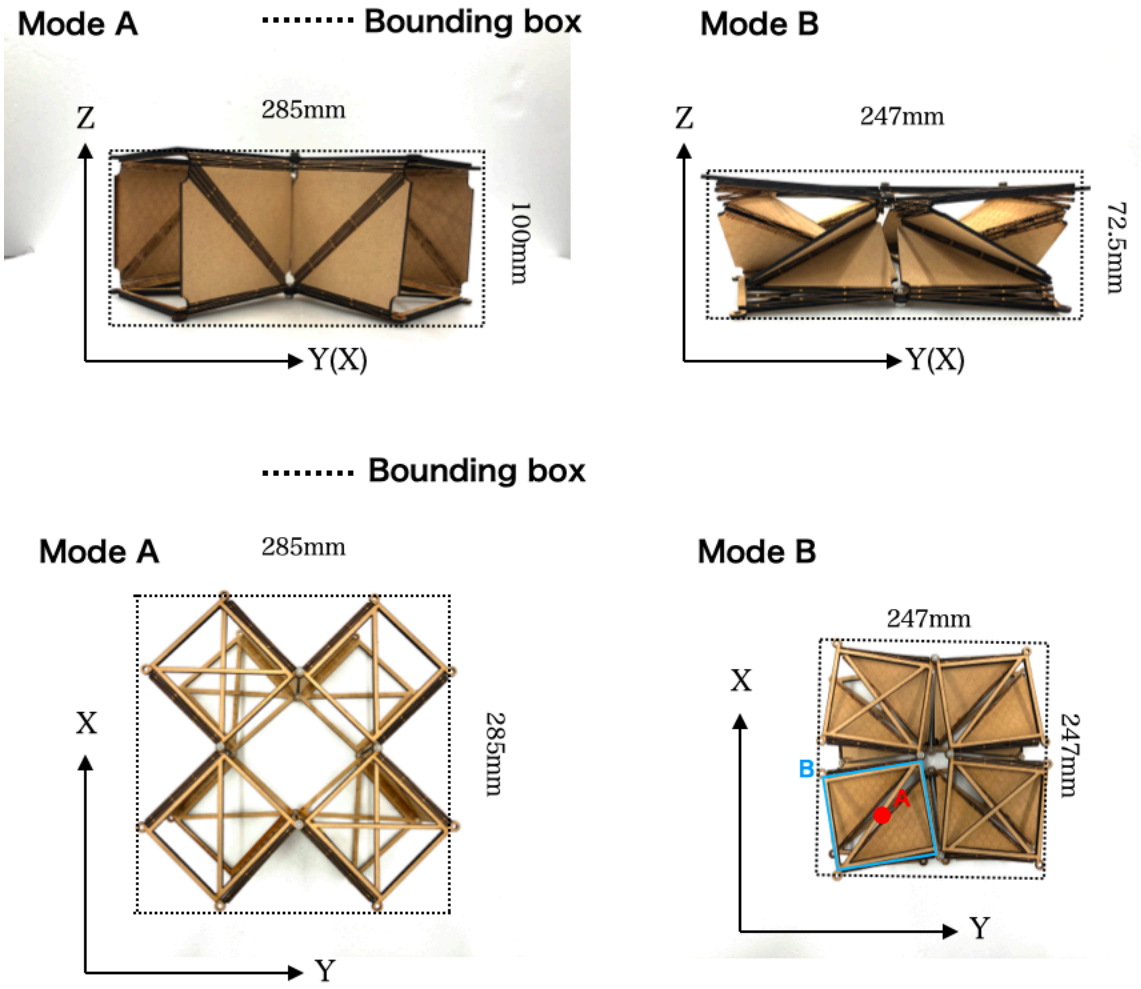


Figure 5.8: Bounding box of the bistable state of this structure.

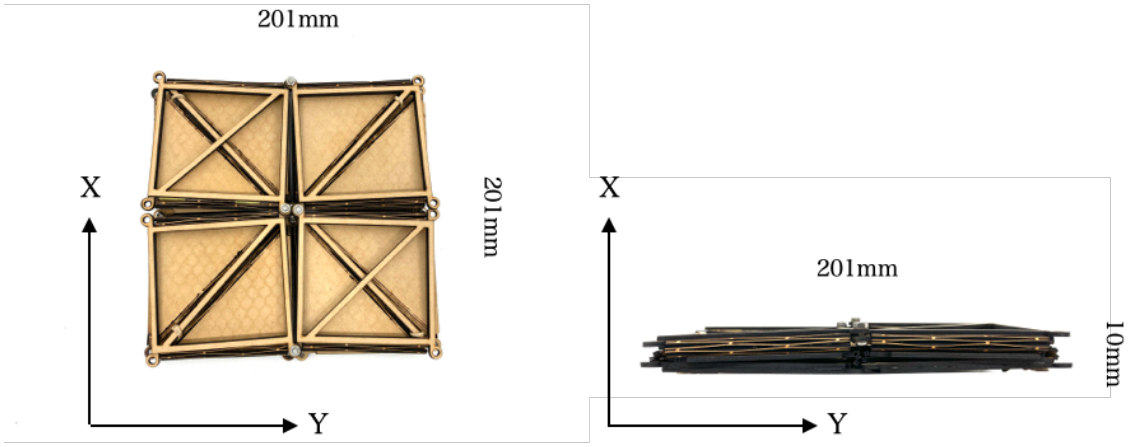


Figure 5.9: This structure is compressed until the rigid materials are in contact with each other.

Figure 5.10: The MDF board is in contact with the surface.

# Chapter 6

# Discussion

In this chapter, we will discuss the results of the analysis and experiments performed in Chapter 5. In Chapter 5, the bistability and Poisson's ratio were obtained based on the load-displacement curve analyzed and experimented, and the trajectory of the structure was recorded by motion capture. Among them, there was a large error between the analysis value and the experiment especially in the load displacement curve. In this chapter, we will also discuss the evaluation of this structure centering on the load displacement curve.

## 6.1 Load Displacement Curve

The prominent features of the load-displacement curve obtained in Section 5.1 was shown in Figure 6.1. By observing the difference between the analytical value and the experimental value shown in area A, it can be seen that the entire graph of the experimental value has a lower load than the analysis. It can be seen from the graph that the experimental value is softer than the analysis value when the voxel structure is compressed from above in the Z-axis direction. This structure is realized in the twisted fold with the Ron Resch pattern and LETA, as shown in Chapter 3. In this paragraph, the Ron Resch pattern has a link mechanism in the XY direction, and since the twisting and folding of each voxel constituting this structure has no degree of freedom in the XY direction, it does not interfere with the degree of freedom of the Ron Resch pattern. In other words, the compression reaction force in the Z-axis direction is contributed by torsional folding. As shown in Chapter 3, twisting folds causes bending of the entire structure in the process of fold deformation, which produces half a force. In this structure, the deflection is absorbed by LETA, specifically this LETA produces a reaction force. As shown in Section 3.4, the parameters of the local beams that make up LETA contribute to the overall rigidity of LETA. In this experiment and analysis, the LETA design parameters were set to the same values in both, so it is probable that a manufacturing error occurred in the structure used in the experiment. Thus, we measured the parameters of the local beam of the structure actually used.

Subsequently, the thickness a of the local beam was 0.85 mm as shown in Figure 6.2. Since the parameter at the design stage is 1.4 mm, the thickness of 0.55 mm has disappeared. This is a burnout caused by a laser cutter. A laser cutter is a device that cuts the material by burning the material with a laser, so it can be said to be the thickness of the laser. Thus, considering the thickness of the beam that will be burnt down by the laser, we manufactured a voxel with an actual measurement value of 1.4 mm and obtained a load

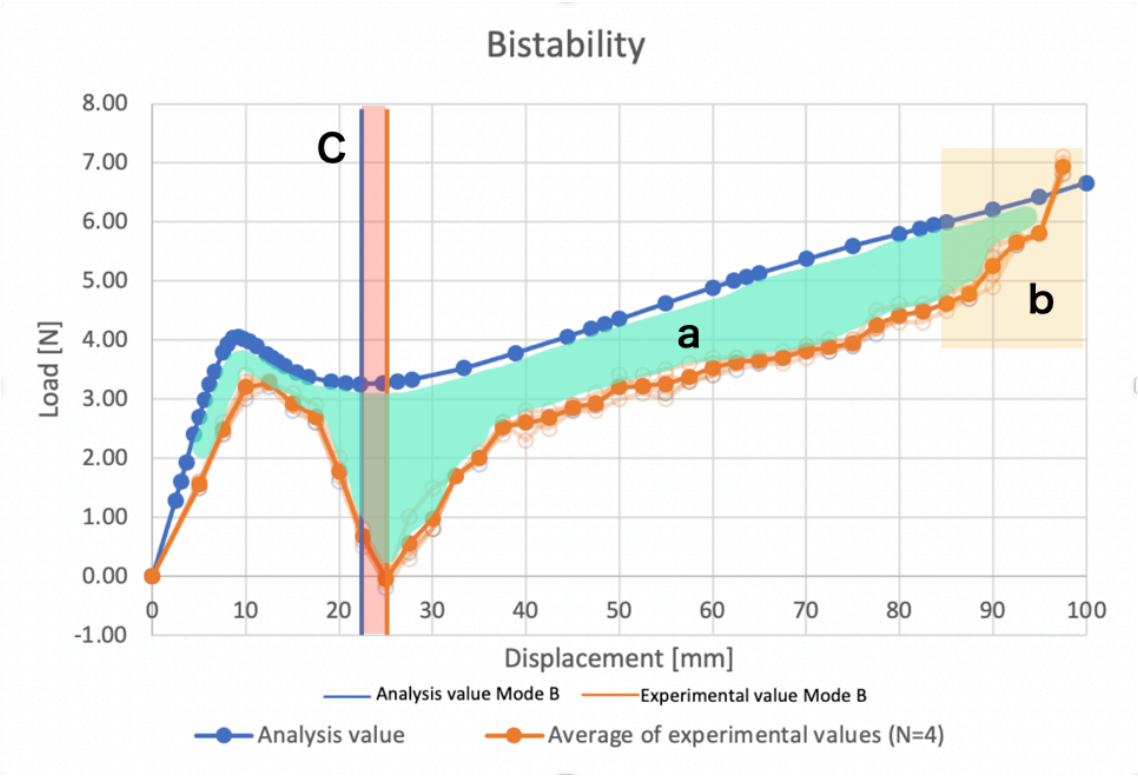


Figure 6.1: The part of the load variation curve to be discussed.


Figure 6.2: Measured local beam thickness of the structure used for the experiment in Chapter 4.

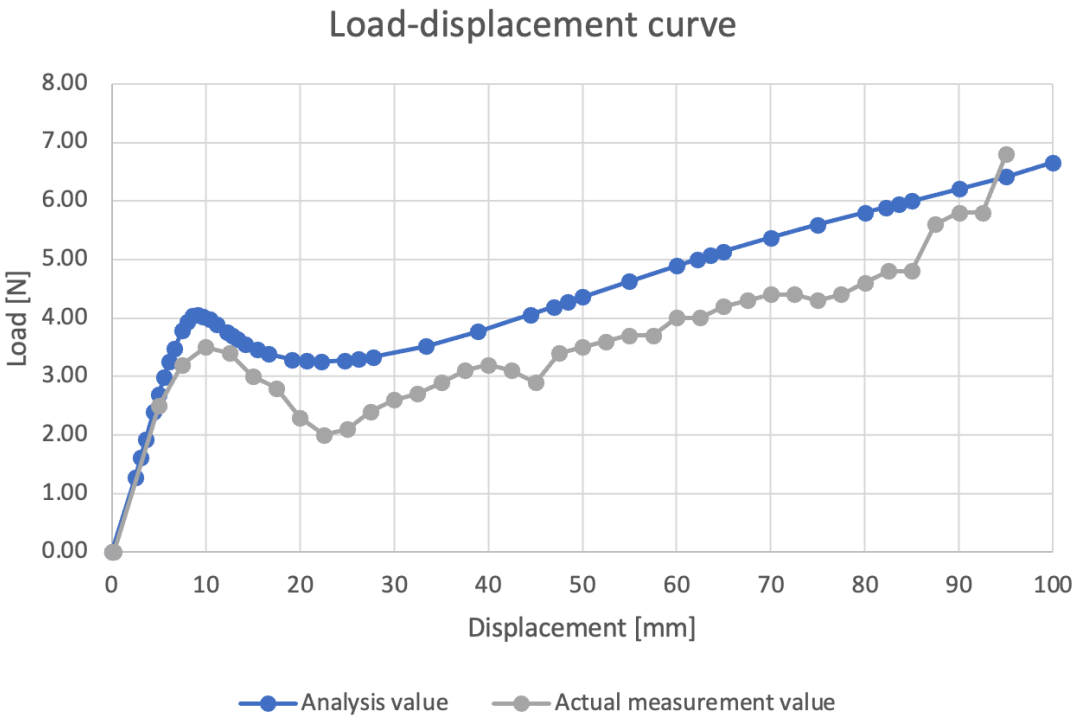


Figure 6.3: Load-displacement curve of LETA based on actual measurements.

displacement curve.

The graph is shown in Figure 6.3. In the graph, the average of the gap band between the measured value and the analyzed value approached 0.91 N. Other possible reasons for the inconsistency in the results of Figure 6.3 are the mass of the material itself and the unevenness of the burnt surface of the beam due to the laser. The actual mass of the material was 50 g. In other words, about 0.49 N is not taken into consideration in this analysis. Furthermore, the burnt surface is not smooth, and there are irregularities due to manufacturing errors, and it is considered that there are some places where the actual beam thickness is thin, although it is a small amount.

Secondly, b in Figure 6.1 will be discussed. In the area b, the slope of the load graph starts to rise sharply when the displacement is around 85 mm. We considered that this is because the boundary condition of the finite element method does not consider the contact of the structure. The contact from 75 mm of the displacement of the structure subjected as shown in Figure 6.4 to the load test.

From 80 mm to 95 mm, the beams of LETAs and the surface of the structure and LETAs are starting to come into contact with each other. When the rigid bodies come into contact with each other, the graph of the load of deformation of the structure evaluates the hardness of the material. On the other hand, since the contact is not considered in the analysis value, the reaction force of LETA is reflected in the graph, and a linear graph appears. This is considered to be the cause of the characteristic of b.

Finally, c in Figure 6.1 will be discussed. The gap between the analysis value and the experimental value of the bistability of c is 2.5 mm in displacement, which is not a large value compared to a and b. However, when considering the effect, it can be considered

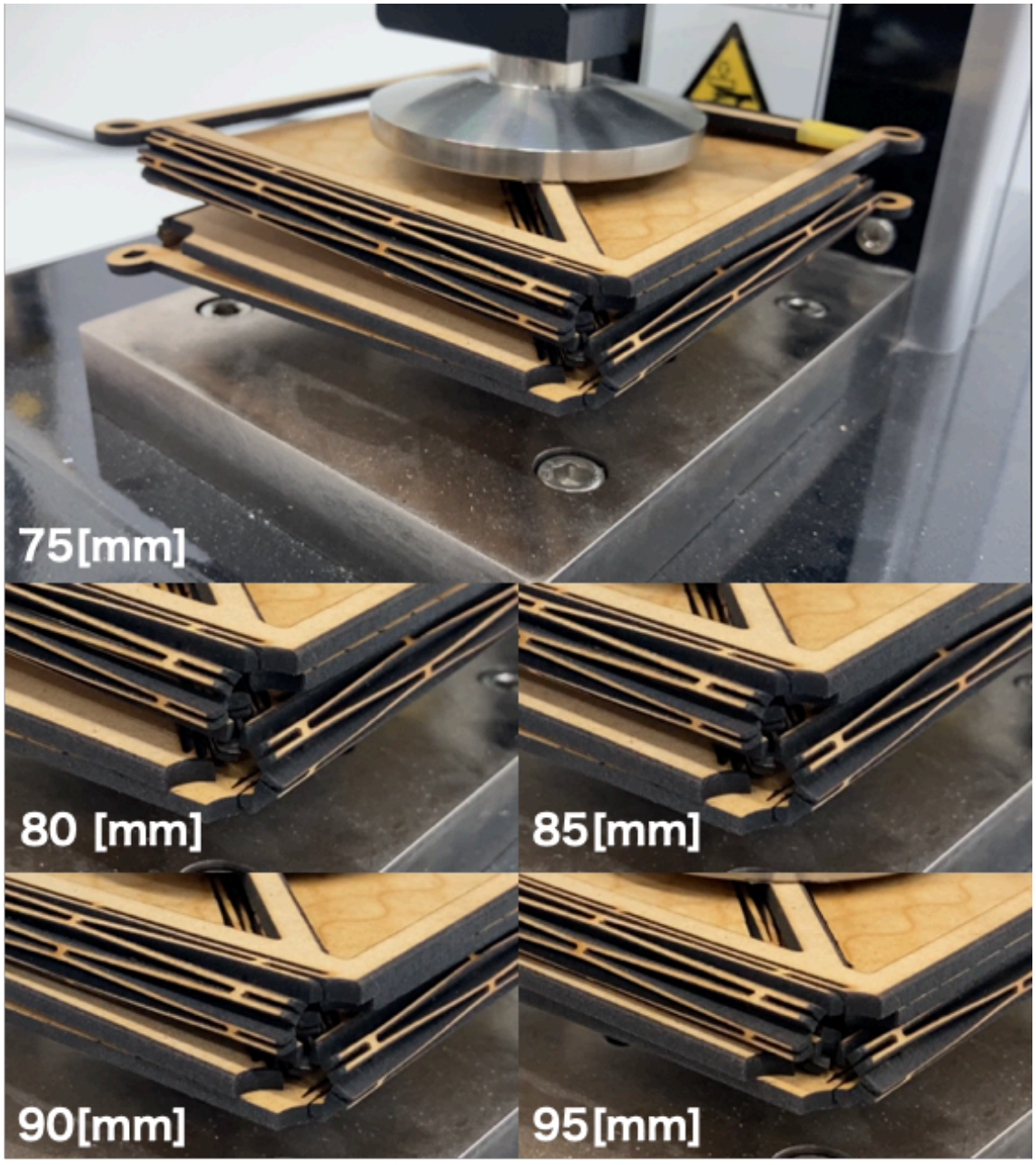


Figure 6.4: Structural contact due to displacement.

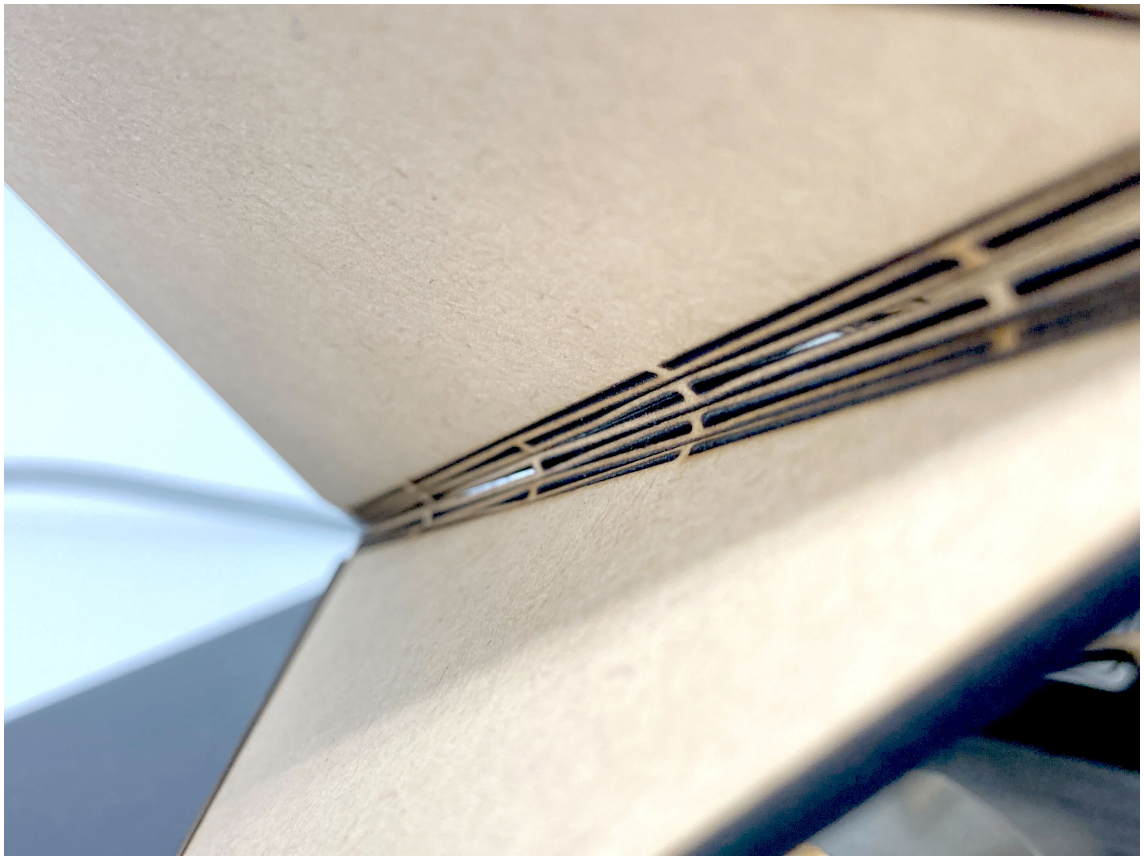

Figure 6.5: Beam collision at displacement of 22.5 mm

that the contact of the LETA beam shown in Figure 6.4 has an effect. With reference to the graph as shown in Figure 6.1, the analysis value shows the lowest value of mode B with a displacement of 22.5 mm. The state of the voxel structure at this time is shown in Figure 6.5. Hence, the contact of the local beams of LETA has already occurred, and it is considered that the friction of the contact between the beams causes an error with respect to the displacement of the bistability.

## 6.2 Application Discussion

In this thesis, we have proposed a three-dimensional auxetic material that can be manufactured by two-dimensional plane processing, however there are some points that must be discussed when actually considering the application of this structure. First is the mechanism of the Ron Resch pattern. In this thesis, one voxel was manufactured on a cubic scale with a side of about 100 mm and evaluated, but the current mechanism mainly limits the reduction of the structural scale. Presently, auxetic materials have emerged in the field of expression, and although the scale of the structures used in those fields is relatively large, they were originally studied on the scale of materials.

Also, in this thesis, the mechanical mechanism is used for deformation, hence, it depends on the axial force of bolts and the like. Also, when viewed from the scale of the entire structure, LETA is also composed of minute beams, however even if the problem of the mechanism is solved, it will be the overall scale on which the establishment of LETA is a prerequisite. Furthermore, due to the mechanical mechanism and the use of LETA, which is an elastic body, there are many degrees of freedom in the entire structure. Even if you deform what you actually manufactured, you can feel the freedom of the entire structure to sway in all directions. On the other hand, in order to actually use the deformed structure such as auxetic material in products, it is desirable that the deformed structure before and after the deformation is fixed. In reality, it is often used by adding a mechanism such as an off-the-shelf product that temporarily holds the deformed state.Under such conditions, the structure has the property of bistability, so that the state of compression and expansion can be fixed.

However, since the appearance of bisstability depends on the reaction force of LETA, it is necessary to optimize the structure for each application with the degree of freedom and bisstability given to the entire structure.

We are considering these points and the application of the characteristics including the scale of the structure realized in this thesis at present, it is considered appropriate that a strong force is not applied from the outside in the expanded state. Since the bounding box of the structure becomes very thin in the compressed state, it is suitable for efficiency of delivery and transportation, also there is a possibility that it can be used as an advertising tower or lighting that expands after delivery to the site.

# Chapter 7

# Conclusion

This paper proposed a model of a three-dimensional auxetic structure that can be manufactured by two-dimensional plane machining.For the structure that realizes the three-dimensional negative Poisson' s ratio that has already been proposed to realize this structure, Chapter 3 propose a model that can be manufactured with a flat surface processing machine so that it can be applied to relatively large buildings and furniture. This structure was used LETA for cylindrical twist folding. LETA is a structure that gives elasticity to the material by inserting a repeated cut pattern. In the case of cylindrical twist folding, it is necessary to absorb the bending in the process of deformation, and it was made possible to deform by inserting LETA into the bent line part of this structure. The structure proposed by LETA by absorbing the deflection has bi-stability, and the structure could be realized only by two-dimensional plane processing. Furthermore, in this paper was evaluated this structure by analyzing and experimenting with the items of load displacement curve, deformation trajectory of structure, Poisson' s ratio, and bistability. The load-displacement curve shows what kind of reaction force is applied to the load in the Z-axis direction of the structure by the LETA parameter. This paper was demonstrate how the rotation of the Ronless pattern affects the displacement of the structure in the Z-axis direction depending on the deformation trajectory of the structure. The Poisson' s ratio and bistability of this structure were also obtained from the experimental and analyzed values of the load-displacement curve. The achieved structure has a high compression ratio and bistability. However, the degree of freedom of LETA as an elastic body generated a degree of freedom in the entire structure.The actual application of this structure will require optimization of the LETA design parameters for the elastic modulus and the degrees of freedom of the entire structure.

# References


[1] Hyeonho Cho, Dongsik Seo, and Do-Nyun Kim. *Mechanics of Auxetic Materials*, pages 733–757. Springer Singapore, Singapore, 2019.

[2] Joseph N Grima and Kenneth E Evans. Auxetic behavior from rotating squares. 2000.

[3] Giles W Hunt and Ichiro Ario. Twist buckling and the foldable cylinder: an exercise in origami. *International Journal of Non-Linear Mechanics*, 40(6):833–843, 2005.

[4] Hiromi Yasuda, Tomohiro Tachi, Mia Lee, and Jinkyu Yang. Origami-based tunable truss structures for non-volatile mechanical memory operation. *Nature communications*, 8(1):1–7, 2017.

[5] Taisuke Ohshima, Tomohiro Tachi, Hiroya Tanaka, and Yasushi Yamaguchi. Analysis and design of elastic materials formed using 2d repetitive slit pattern. In *Proceedings of IASS Annual Symposia*, volume 2015, pages 1–12. International Association for Shell and Spatial Structures (IASS), 2015.

[6] Taisuke Ohshima, Tomohiro Tachi, Hiroya Tanaka, and Yasushi Yamaguchi. Analysis and design of elastic materials formed using 2d repetitive slit pattern. In *Proceedings of IASS Annual Symposia*, volume 2015, pages 1–12. International Association for Shell and Spatial Structures (IASS), 2015.

[7] Beach. A simpler approach to auxetic package design). `https://beachpackagingdesign.com/boxvox/a-simpler-approach-to-auxetic-package-design1`, 2017. (Accessed on December 23, 2021).

[8] Roderic Lakes. Foam structures with a negative poisson's ratio. *Science*, 235:1038–1041, 1987.

[9] Ken E Evans. Auxetic polymers: a new range of materials. *Endeavour*, 15(4):170–174, 1991.

[10] Shengyu Duan, Li Xi, Weibin Wen, and Daining Fang. A novel design method for 3d positive and negative poisson's ratio material based on tension-twist coupling effects. *Composite Structures*, 236:111899, 2020.

[11] Yanping Liu and Hong Hu. A review on auxetic structures and polymeric materials. *Scientific Research and Essays*, 5(10):1052–1063, 2010.

[12] A.G. Kolpakov. Determination of the average characteristics of elastic frameworks. *Journal of Applied Mathematics and Mechanics*, 49(6):739–745, 1985.

[13] George Neville Greaves, AL Greer, Roderic S Lakes, and Tanguy Rouxel. Poisson's ratio and modern materials. *Nature materials*, 10(11):823–837, 2011.

[14] Kenneth E Evans and Andrew Alderson. Auxetic materials: functional materials and structures from lateral thinking! *Advanced materials*, 12(9):617–628, 2000.

[15] IG Masters and KE Evans. Models for the elastic deformation of honeycombs. *Composite structures*, 35(4):403–422, 1996.

[16] Chris W Smith, JN Grima, and KenE Evans. A novel mechanism for generating auxetic behaviour in reticulated foams: missing rib foam model. *Acta materialia*, 48(17):4349–4356, 2000.

[17] Roderic Lakes. Foam structures with a negative poisson's ratio. *Science*, 235:1038–1041, 1987.

[18] Stephen Burns. Negative poisson's ratio materials. *Science*, 238(4826):551–551, 1987.

[19] Ulrik Darling Larsen, O Signund, and S Bouwsta. Design and fabrication of compliant micromechanisms and structures with negative poisson's ratio. *Journal of microelectromechanical systems*, 6(2):99–106, 1997.

[20] Chris W Smith, JN Grima, and KenE Evans. A novel mechanism for generating auxetic behaviour in reticulated foams: missing rib foam model. *Acta materialia*, 48(17):4349–4356, 2000.

[21] Neil Gaspar, XJ Ren, Chris W Smith, JN Grima, and Ken E Evans. Novel honeycombs with auxetic behaviour. *Acta Materialia*, 53(8):2439–2445, 2005.

[22] Li Yang, Ola Harrysson, Harvey West, and Denis Cormier. Compressive properties of ti–6al–4v auxetic mesh structures made by electron beam melting. *Acta Materialia*, 60(8):3370–3379, 2012.

[23] Roderic Lakes. Deformation mechanisms in negative poisson's ratio materials: structural aspects. *Journal of materials science*, 26(9):2287–2292, 1991.

[24] Andrew Alderson, KL Alderson, G Chirima, N Ravirala, and KM Zied. The in-plane linear elastic constants and out-of-plane bending of 3-coordinated ligament and cylinder-ligament honeycombs. *Composites Science and Technology*, 70(7):1034–1041, 2010.

[25] Chan Soo Ha, Michael E Plesha, and Roderic S Lakes. Chiral three-dimensional lattices with tunable poisson' s ratio. *Smart Materials and Structures*, 25(5):054005, 2016.

[26] Joseph N Grima and Kenneth E Evans. Auxetic behavior from rotating squares. 2000.

[27] Joseph N Grima, Ruben Gatt, Andrew Alderson, and Kenneth E Evans. On the auxetic properties of 'rotating rectangles' with different connectivity. *Journal of the Physical Society of Japan*, 74(10):2866–2867, 2005.

[28] Alex Slann, William White, Fabrizio Scarpa, Katarzyna Boba, and Ian Farrow. Cellular plates with auxetic rectangular perforations. *physica status solidi (b)*, 252(7):1533–1539, 2015.

[29] Joseph N Grima, Andrew Alderson, and Kenneth E Evans. An alternative explanation for the negative poisson' s ratios in auxetic foams. *Journal of the Physical Society of Japan*, 74(4):1341–1342, 2005.

[30] Daphne Attard and Joseph N Grima. Auxetic behaviour from rotating rhombi. *physica status solidi (b)*, 245(11):2395–2404, 2008.

[31] Daphne Attard, Elaine Manicaro, and Joseph N Grima. On rotating rigid parallelograms and their potential for exhibiting auxetic behaviour. *physica status solidi (b)*, 246(9):2033–2044, 2009.

[32] Cagdas D Onal, Robert J Wood, and Daniela Rus. An origami-inspired approach to worm robots. *IEEE/ASME Transactions on Mechatronics*, 18(2):430–438, 2012.

[33] Je-sung Koh, Sa-reum Kim, and Kyu-jin Cho. Self-folding origami using torsion shape memory alloy wire actuators. In *International Design Engineering Technical Conferences and Computers and Information in Engineering Conference*, volume 46377, page V05BT08A043. American Society of Mechanical Engineers, 2014.

[34] Kaori Kuribayashi, Koichi Tsuchiya, Zhong You, Dacian Tomus, Minoru Umemoto, Takahiro Ito, and Masahiro Sasaki. Self-deployable origami stent grafts as a biomedical application of ni-rich tini shape memory alloy foil. *Materials Science and Engineering: A*, 419(1-2):131–137, 2006.

[35] Stefan Marinitsch, Christian Schranz, and Martien Teich. Folded plate structures made of glass laminates: a proposal for the structural assessment, 2016.

[36] National Aeronautics and Space Administration. Solar power, origami-style. `https://www.nasa.gov/jpl/news/origami-style-solar-power-20140814`, 2014. (Accessed on December 23, 2021).

[37] ISSEI MIYAKE. 132 5. `https://www.isseymiyake.com/ja/brands/1325`, 2010. (Accessed on December 23, 2021).

[38] Vincenzo Sapienza and Gianluca Rodonò. Kinetic architecture and foldable surface. *Athens J. Archit*, 2:223–235, 2016.

[39] Wyss Institute. Pop-up mems: Origami-inspired micromanufacturing. `https://wyss.harvard.edu/technology/pop-up-mems-origami-inspired-micromanufacturing/`, 2020. (Accessed on December 23, 2021).

[40] John Rogers, Yonggang Huang, Oliver G Schmidt, and David H Gracias. Origami mems and nems. *Mrs Bulletin*, 41(2):123–129, 2016.

[41] Tomohiro Tachi. *6. Freeform Rigid-Foldable Structure Using Bidirectionally Flat-Foldable Planar Quadrilateral Mesh*. Ambra Verlag, 2016.

[42] 野島武敏. 平板と円筒の折りたたみ法の折紙によるモデル化. **日本機械学会論文集** *C* **編**, 66(643):1050–1056, 2000.

[43] Yoshimaru Yoshimura. On the mechanism of buckling of a circular cylindrical shell under axial compression. Technical report, 1955.

[44] Xin TAO Ichiro HAGIWARA*5, Chihiro YAMAMOTO and Taketoshi NOJIMA. Optimization for crush characteristics of cylindrical origami structure using reversed spiral model. **日本機械学会論文集** *A* **編**, 70(689):36–42, 2004.

[45] 趙希禄, 胡亜波, and 萩原一郎. 折紙工学を利用した円筒薄肉構造物の衝突圧潰特性の最適設計. **日本機械学会論文集** *A* **編**, 76(761):10–17, 2010.

[46] Noboru Yamaki. *Elastic stability of circular cylindrical shells*. Elsevier, 1984.

[47] Hiromi Yasuda, Tomohiro Tachi, Mia Lee, and Jinkyu Yang. Origami-based tunable truss structures for non-volatile mechanical memory operation. *Nature communications*, 8(1):1–7, 2017.

[48] WEsearch Lab. Waffle structure as canopy at ahmedabad by wesearch lab). `https://architecturelive.in/waffle-structure-as-canopy-at-ahmedabad-by-wesearch-lab/`, 2018. (Accessed on December 23, 2021).

[49] John Edmark. Curling spiral (outer spine). `http://www.johnedmark.com/spirals1`, 2011. (Accessed on December 23, 2021).

[50] Bryce P DeFigueiredo, Trent K Zimmerman, Brian D Russell, and Larry L Howell. Regional stiffness reduction using lamina emergent torsional joints for flexible printed circuit board design. *Journal of Electronic Packaging*, 140(4), 2018.

[51] Todd G Nelson, Robert J Lang, Nathan A Pehrson, Spencer P Magleby, and Larry L Howell. Facilitating deployable mechanisms and structures via developable lamina emergent arrays. *Journal of Mechanisms and Robotics*, 8(3):031006, 2016.